Mobility Modeling

Prepared by:

Dragica Vasileska
Associate Professor

Arizona State University

Mobility Modeling and Characterization

Electrons and holes are accelerated by the electric fields, but lose momentum as a result of various scattering processes. These scattering mechanisms include lattice vibrations (phonons), impurity ions, other carriers, surfaces, and other material imperfections. A detailed chart of most of the imperfections that cause the carrier to scatter in a semiconductor is given in Figure 1.

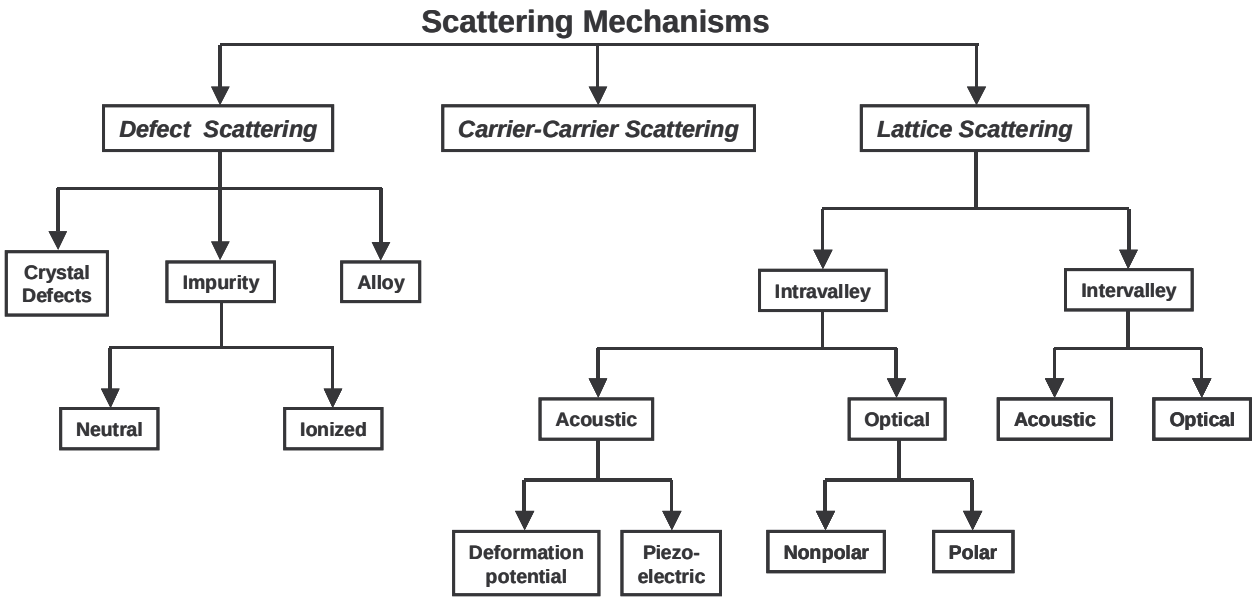

Figure 1. Scattering mechanisms in a typical semiconductor.

Since the effects of all of these microscopic phenomena are lumped into the macroscopic mobilities introduced by the transport equations, these mobilities are therefore functions of the local electric field, lattice temperature, doping concentration, and so on. Mobility modeling is normally divided into: (i) low field behavior, (ii) high field behavior, (iii) bulk semiconductor regions and (iv) inversion layers. The low electric field behavior has carriers almost in equilibrium with the lattice and the mobility has a characteristic low-field value that is commonly denoted by the symbol $\mu_{n0,p0}$. The value of this mobility is dependent upon phonon and impurity scattering, both of which act to decrease the low field mobility. The high electric field behavior shows that the carrier mobility declines with electric field because the carriers that

gain energy can take part in a wider range of scattering processes. The mean drift velocity no longer increases linearly with increasing electric field, but rises more slowly. Eventually, the velocity does not increase any more with increasing field, but saturates at a constant velocity. This constant velocity is commonly denoted by the symbol v_{sat}. Impurity scattering is relatively insignificant for energetic carriers, and so v_{sat} is primarily a function of the lattice temperature.

In the early days, most experimental work on inversion layer mobilities has concentrated on *Hall* and *field-effect* mobilities. However, it is the *effective* mobility which appears in all theoretical models of MOS transistors and which is, therefore, most useful in modern MOS device modeling. Of lesser importance is the so-called *saturation* mobility. The Hall mobility, described in section 1(a), represents the bulk mobility and the interface, as well as the quantization effect, plays a minor role in its determination. The field-effect, effective and saturation mobilities, used to characterize MOSFET's, are described in section 1(b). The mobility models used in prototypical device simulator are categorized in section 2.

1 Experimental Mobilities

1.a) Hall mobility

The Hall measurement technique is commonly used for resistivity measurements, carrier concentration characterization as well as mobility measurements. The basic setup of the Hall technique is given in Fig. 1. As shown in the figure, the applied electric field along the *x*-axis gives rise to a current I_x. The Lorentz force $F_y = ev_x B_z$ due to the applied magnetic field along the positive *z*-axis pushes the carriers upwards. This results in a pile up of electrons and holes at the top part of the sample which, in turn, gives rise to electric fields E_{yn} and E_{yp}, respectively. The transverse electric fields along the *y*-axis are called *Hall fields*. Since there is no net current along the *y*-direction in steady-state, the induced electric fields along the *y*-axis exactly balance the Lorentz force, i.e.

$$\frac{V_H}{w} = R_H J_x B_z \ . \tag{1}$$

In (1), J_x is the current density and R_H is the so-called Hall coefficient. If both electrons and holes are present in the sample, the Hall coefficient is given by

$$R_H = \frac{r_h p - r_e b^2 n}{e(p + bn)^2} \ , \tag{2}$$

where $n\,(p)$ is the electron(hole) concentration, $b = \mu_e/\mu_h$ is the mobility ratio and r_e (r_h) is the so-called Hall scattering factor for electrons (holes) that takes into account the energy spread of the carriers. The Hall scattering factor that appears in (2), is defined by the ratio

$$r = \frac{\langle \tau^2 \rangle}{\langle \tau \rangle^2} \ , \tag{3}$$

where τ is the mean-free time between carrier collisions, and the average value of the *m*th power of τ in *d*-dimensions is calculated from

$$\langle \tau^m \rangle = \frac{\int_0^\infty \varepsilon^{d/2} \tau^m(\varepsilon)(\partial f_0/\partial \varepsilon) d\varepsilon}{\int_0^\infty \varepsilon^{d/2}(\partial f_0/\partial \varepsilon) d\varepsilon} \ , \tag{4}$$

where f_0 is the equilibrium Fermi-Dirac distribution function.

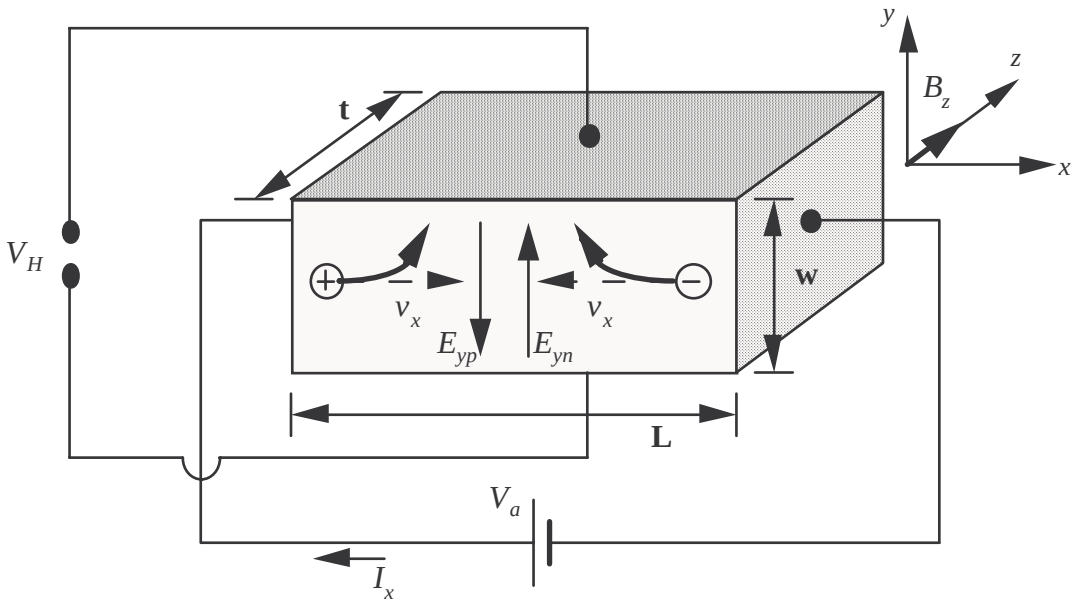

Figure 1 Experimental setup for Hall measurement technique.

The Hall mobility μ_H is defined as a product of the Hall coefficient R_H and conductivity σ_x

$$\mu_H = |R_H| \sigma_x \ , \tag{5}$$

which is calculated from

$$\sigma_x = \frac{I_x L}{wtV_a} \ . \tag{6}$$

It is important to point out that the Hall mobility has to be distinguished from the so-called conductivity (or effective) mobility which does not contain the Hall scattering factor. The two mobilities are related to each other according to

$$\mu_H = r\mu_{eff} \ . \tag{7}$$

1.b) MOSFET Mobilities

Electron mobility in surface-inversion layers has been of considerable interest for many years. At present, several mobilities (already mentioned in the introduction part of this appendix) are used to characterize MOSFETs [1].

The *effective mobility* μ_{eff} is usually deduced from the first-order one-dimensional model in the linear mode. At low drain voltages ($V_{DS} = 10 - 50mV$, where $V_{DS} << V_{GS} - V_T$), the effective mobility is related to the *drain conductance*

$$g_D = \left. \frac{\partial I_D}{\partial V_{DS}} \right|_{V_{GS}=const.} \ , \tag{8}$$

according to

$$\mu_{eff} \approx \frac{Lg_D}{ZC_{ox}\left(V_{GS} - V_T\right)} \ . \tag{9}$$

In expressions (8) and (9), I_D is the drain current, L is the length and Z is the width of the channel, V_{GS} is the gate voltage, and V_T is the so-called threshold gate voltage. The threshold gate voltage is often defined as the voltage where the Fermi level is as close to the conduction (or valence) band at the surface as to the valence (or conduction) band in the bulk. It is experimentally determined by using various linear extrapolation techniques on the $I_D - V_{GS}$ curves, as explained in [**Error! Bookmark not defined.**]. The inaccuracies in the threshold

voltage significantly affect the effective mobility results. Both thermal broadening and trapping tend to obscure the accurate measurements of V_T and, therefore, μ_{eff}.

The previously described effective mobility is distinct from the so-called *field-effect mobility* μ_{FE} which is obtained from the MOSFET *transconductance*

$$g_m = \left.\frac{\partial I_D}{\partial V_{GS}}\right|_{V_{DS}=const.} \tag{10}$$

through the expression

$$\mu_{FE} = \frac{L g_m}{Z C_{ox} V_{DS}} \ . \tag{11}$$

The experimentally measured field-effect mobility is usually smaller than the effective mobility. The discrepancy between the effective and field-effect mobility is associated with the neglect of the electric-field dependence (more precisely, the neglect of the gate voltage dependence) in the derivation of the expression for μ_{FE}. For example, for the device in the linear regime and using the definitions given in (8) and (10), after a straightforward calculation it follows that the two mobilities can be related to each other according to

$$\mu_{FE} \approx \mu_{eff} + \left(V_{GS} - V_T\right)\left.\frac{\partial \mu_{eff}}{\partial V_{GS}}\right|_{V_{DS}=const.} \ . \tag{12}$$

Since the effective mobility decreases with the gate voltage, i.e. $\partial \mu_{eff} / \partial V_{GS} < 0$ (except for very low gate voltages, where it actually increases due to the decreased importance of Coulomb scattering), $\mu_{FE} < \mu_{eff}$. Therefore, if μ_{FE} is used for device modeling, the currents and device switching speeds are going to be underestimated.

Very rarely, the MOSFET mobility is obtained from the output current-voltage characteristics with the device in saturation. In this regime, the saturation drain current $I_{D,sat}$ is calculated from

$$I_{D,sat} = \frac{B Z \mu_{sat} C_{ox}}{2L}\left(V_{GS} - V_T\right)^2, \tag{13}$$

where B is the body factor, which is not always well known. If one plots the variation of $\sqrt{I_{D,sat}}$ vs. $\left(V_{GS} - V_T\right)$, then the so-called *saturation mobility* is determined from the slope *m* of this curve, according to

$$\mu_{sat} = \frac{2Lm^2}{BZC_{ox}} \ . \tag{12}$$

Again, due to the neglect of the gate-voltage dependence in the definition for the saturation mobility, the experimental results for μ_{sat} are always smaller compared to the ones obtained for μ_{eff}.

2 Mobility Modeling

As already noted, mobility modeling is normally divided into: (1) low- and high-field behavior, and (2) bulk semiconductor regions and inversion layers. Mobility models fall into one three broad categories: physically-based, semi-empirical, and empirical. Physically-based models are those that are obtained from a first-principles calculation, i.e. both the coefficients and the power dependencies appearing in the model are obtained from a fundamental calculation. In practice, physically-based models rarely agree with experimental data since considerable simplifying assumptions are made in order to arrive at a closed form solution. Therefore, to reconcile the model with experimental data, the coefficients appearing in the physically-based model are allowed to vary from their original values. In this process the power-law dependencies resulting from the first-principles calculation are preserved, and the resulting model is termed as semi-empirical. At the other end of the spectrum are empirically-based models in which the power-law dependencies are also allowed to vary. Empirical models have less physical content compared to the other two models, and also exhibit a narrower range of validity. Empirical models are usually resorted to when the dependencies predicted by the first-principles calculation do not allow a good fit between the experimental data and the corresponding semi-empirical model.

At low-fields and bulk samples carriers are almost in equilibrium with the lattice vibrations and the low-field mobility is mainly affected by phonon and Coulomb scattering. At higher electric fields mobility becomes field-dependent parameter and it decreases with increasing electric field due to increased lattice scattering at higher carrier energies. In general, the bulk mobility modeling is a three-step procedure:

- Characterize low field mobility μ_0 as a function of doping and lattice temperature *T*.
- Characterize the saturation velocity v_{sat} as a function of the temperature *T*.
- Describe the transition between the low-field and high-field regions.

Modeling carrier mobilities in inversion layers introduces additional complications. Carriers in inversion layers are subject to surface scattering, extreme carrier-carrier scattering, and quantum-mechanical size quantization effects. These effects must be accounted for in order to perform accurate simulation of MOS devices. The transverse electric field is often used as a parameter that indicates the strength of inversion layer phenomena. It is possible to define multiple non-conflicting mobility models simultaneously. It is also necessary to know which models are over-riding when conflicting models are defined.

The low-field mobility models for bulk materials include:

- constant mobility model
- Caughey and Thomas model (doping and temperature dependent mobilities) [2]
- Arora model (includes doping and temperature dependence) [3]
- Dorkel-Leturg model (includes dependence on temperature, doping and carrier-carrier scattering) [4]
- Klaassen unified low-field mobility model (provides unified description of majority and minority carrier mobility. In doing so, it includes the effects of lattice scattering, screened Coulomb charges, carrier-carrier scattering and impurity clustering effects at high concentrations) [5]

To obtain accurate results for MOSFET simulations, it is necessary to account for the mobility degradation that occurs inside inversion layers. The degradation normally occurs as a result of the substantially higher surface scattering near the semiconductor to insulator interface. This effect is handled within ATLAS by three distinct methods:

- a surface degradation model SURFMOB
- a transverse electric field model SHIRAHATA [6]
- specific inversion layer mobility models CVT (Lombardi) [7], YAMAGUCHI [8] and TASCH [9]

The CVT, YAMAGUCHI and TASCH models are designed as stand-alone models which incorporate all the effects required for simulating the carrier mobility.

As carriers are accelerated in an electric field their velocity will begin to saturate at high enough electric fields. This effect has to be accounted for by a reduction of the effective mobility since the magnitude of the drift velocity is the product of the mobility and the electric field component in the direction of the current flow. The following Caughey and Thomas expression [10] is usually used to implement a field-dependent mobility that provides a smooth transition between low-field and high field behavior:

$$\mu_n(E) = \mu_{n0}\left[1+\left(\frac{\mu_{n0}E}{v_{sat}^n}\right)^{\beta_n}\right]^{-1/\beta_n} \tag{13}$$

$$\mu_p(E) = \mu_{p0}\left[1+\left(\frac{\mu_{p0}E}{v_{sat}^p}\right)^{\beta_p}\right]^{-1/\beta_p} \tag{14}$$

where E is the parallel electric field and μ_{n0} and μ_{p0} are the low field electron and hole mobilities respectively. The low field mobilities are either set explicitly on the `MOBILITY` statement or calculated by one of the low field mobility models. The model parameters $\beta_n = 2$ (`BETAN`) and $\beta_p = 1$(BETAP) are user definable on the `MOBILITY` statement. The saturation velocities are calculated by default from the temperature dependent model [11]:

$$v_{sat}^n = v_{sat}^p = \frac{2.4\times10^7}{1+0.8\exp\left(\frac{T_L}{600}\right)} \quad [cm/s] \tag{15}$$

but can be set to constant values on the `MOBILITY` statement in Silvaco ATLAS using the parameters `VSATN` and `VSATP`. In this case no temperature dependence is implemented. Specifying the `FLDMOB` parameter on the `MODELS` statement of the Silvaco ATLAS simulation software invokes the field-dependent mobility. `FLDMOB` should always be specified unless one of the inversion layer mobility models (which incorporate their own dependence on the parallel field) are specified.

References

1 D. K. Schroder, Modular Series on Solid State Devices: *Advanced MOS Devices* (Addison-Wesley Publishing Company, New York, 1987).

2 D.M. Caughey, R.E. Thomas, “Carrier mobilities in silicon empirically related to doping and field”, *Proc. IEEE*, Vol. 55, pp 2192-2193 (1967).

3 N.D.Arora, J.R.Hauser, D.J.Roulston, “Electron and hole mobilities in silicon as a function of concentration and temperature”, *IEEE Trans. Electron Devices*, Vol. 29, pp 292-295 (1982).

4 J. M. Dorkel and PH. Leturcq, “Carrier Mobilities in Silicon Semi-Empirically Related to Temperature, Doping and Injection Level”, *Solid-State Electronics*, Vol. 24, pp. 821-825 (1981)

5 D. B. M. Klaassen, “A Unified Mobility Model for DeviceSimulation – I. Model Equations and Concentration Dependence”, *Solid-State Electronics*, Vol. 35, pp. 953-959 (1992).

6 M. Shirahata, H. Kusano, N. Kotani, S. Kusanoki, Y. Akasaka, “A Mobility Model Including the Screening Effect in MOS Inversion Layer”, *IEEE Trans. Comp. Aided Design*, Vol. 11, pp. 1114-1119 (1988).

7 C. Lombardi, S. Manzini, A. Saporito and M. Vanzi, “A Physically Based Mobility Model for Numerical Simulation of Nonplanar Devices”, *IEEE Trans. Comp. Aided Design*, Vol. 7, pp. 1154-1171 (1992).

8 Ken Yamaguchi, “Field-Dependent Mobility Model for Two-Dimensional Numerical Analysis of MOSFET's,” IEEE Trans. Electron Devices, Vol. 26, pp. 1068-1074 (1979).

9 G. M. Yeric, A. F. Tasch, and S. K. Banerjee, “A Universal MOSFET Mobility Degradation Model for Circuit Simulation”, *IEEE Trans. Computer-Aided Design*, Vol. 9, p. 1123 (1991).

10 D. M. Caughey and R. E. Thomas, “Carrier Mobilities in Silicon Empirically Related to Doping and Field”, *Proc. IEEE*, Vol. 55, pp. 2192-2193 (1967).

11 Silvaco ATLAS User Manual.